

Relation between Structure, Mechanical and Piezoelectric Properties in Cellular Ceramic Auxetic and Honeycomb Structures

David Köllner, Swantje Simon, Sebastian Niedermeyer, Isabella Spath, Edwyn Wolf, Ken-ichi Kakimoto, and Tobias Fey*

Optimizing renewable energy harvesting is of major importance in the following decades. In order to increase performance and efficiency, an ideal balance of mechanical and piezoelectric properties must be targeted. For this purpose, the approach of ceramic auxetic and honeycomb structures made of $(\text{Ba,Ca})(\text{Zr,Ti})\text{O}_3$ (BCZT) which is produced via injection molding is considered. The main design parameter is the structural angle θ which is varied between -35° and 35° . Its effect on compressive strength, Young's modulus, and Poisson's ratio are determined via uniaxial compression tests and digital image correlation (DIC). Maximum compressive strength of 95 MPa at 0° (porosity of 59%) is found, which is superior to conventional porous ceramics of the same porosity. The piezoelectric constants d_{33} (max. 296 pC N^{-1}) and g_{33} (max. 0.068 Vm N^{-1}) are measured via the Berlincourt method and also exceed expectations, regardless of the structure. The theoretical models of Gibson and Ashby (mechanical) and Okazaki (piezoelectrical), as well as finite element method simulations, strengthen and explain the experimental results.

properties.^[1–3] Compared to dense piezoelectric ceramics, they show improved signal-to-noise ratio, reduced acoustic impedance to an ambient medium, and higher sensitivity.^[4] Therefore they are optimal for ultrasound transducers, especially in the medical field for sensing or prosthetic interfaces.^[5,6] Furthermore, some studies about bone tissue engineering have already shown that piezoelectric cellular structures have improved bone cell adhesion and proliferation as well as an antibacterial response.^[6–8] Many of these applications are based on foams with randomly distributed cell structures, which exhibit microcracks and sensitive hollow struts that significantly reduce the mechanical properties.^[9,10]

In general, the properties of cellular ceramics are influenced by porosity, connectivity, pore size, shape and morphology, orientation, and distribution. Thus, mechanical

properties such as Young's modulus and compressive strength decrease exponentially with increasing porosity, whereas piezoelectric properties such as large signal d_{33}^* and small-signal d_{33} and d_{31} decrease linearly.^[9–13] At the same time, the relative permittivity falls with increasing porosity, leading to an increased voltage coefficient ($g_h = d_h/\epsilon_{33}$) and an enhanced HFOM.^[11,13–15]

What has been less studied and understood until now is how mechanical and piezoelectric properties influence each other. It is known that Young's modulus can be affected by polarization,^[16] while polarization^[17] or depolarization^[18] can occur by applying a mechanical field. In contrast, Young's modulus and the piezoelectric coefficients are generally separated, as can be seen in Equation (1)^[19]

$$\epsilon_{ij} = S_{ij} * \sigma_{ij} + d_{ij} * E_i \quad (1)$$


Honeycombs represent a subgroup of cellular ceramics, in which the mechanical and piezoelectric properties are strongly controlled by geometrical parameters and less by the porosity itself.^[20,21] Using auxetic PZT lattices (inverse honeycombs), Fey et al. have already shown that despite a porous structure, higher piezoelectric coefficients and strain amplification can be achieved compared to the bulk material.^[22] Furthermore, Tang et al. demonstrated improved piezoelectric properties with an auxetic metamaterial.^[23,24] This is contrary to the fact that the

1. Introduction

Cellular piezoelectric ceramics are of interest in the fields of energy harvesting, hydrophones, sensors, or biomedical implants, because of the very specific requirements of low density, a high hydrostatic figure of merit ($\text{HOFM} = d_h * g_h$), or increased permeability, coupled with suitable mechanical

D. Köllner, S. Simon, S. Niedermeyer, I. Spath, E. Wolf, T. Fey
Department of Materials Science and Engineering (Institute of Glass and Ceramics)
Friedrich-Alexander-Universität Erlangen-Nürnberg
Martensstr. 5, D-91058 Erlangen, Germany
E-mail: tobias.fey@fau.de

K. Kakimoto, T. Fey
Frontier Research Institute for Materials Science
Nagoya Institute of Technology
Gokiso-cho, Showa-ku, Nagoya 466-8555, Japan

 The ORCID identification number(s) for the author(s) of this article can be found under <https://doi.org/10.1002/adem.202201387>.

© 2022 The Authors. Advanced Engineering Materials published by Wiley-VCH GmbH. This is an open access article under the terms of the Creative Commons Attribution License, which permits use, distribution and reproduction in any medium, provided the original work is properly cited.

DOI: 10.1002/adem.202201387

piezoelectric properties are reduced with increasing porosity. It is unclear whether the piezoelectric properties are influenced only by the shape or by the mechanical properties per se.^[22,25–27] The honeycomb lattice has a significantly lower structural Young's modulus than the bulk material. Therefore, the cellular structure has less resistance against deformation. With the same piezoelectric properties, strain amplification would occur, influenced by Young's modulus especially, which can be tailored by the geometry of the honeycomb.^[28–30] For this reason, auxetic and honeycomb structures with different geometries by variation of structural angle θ are produced in this work to investigate the influence of the effective mechanical properties on the piezoelectric properties.

Most current applications are based on lead-containing perovskite lead zirconium titanate (PZT), which must be replaced due to environmental and sustainability considerations.^[31] In addition, medical and biological applications must use lead-free alternatives. The most common and promising alternatives are (K,Na)NbO₃ (KNN), (Ba,Ca)(Zr,Ti)O₃ (BCZT), and (Bi_{0.5}Na_{0.5})TiO₃-BaTiO₃ (BNT-BT)-based systems.^[32–34] In particular, BCZT is a highly flexible material that can be used as a capacitor, energy storage, harvesting, catalytic, sensor, or actuator material,^[35–39] as higher d_{33} values (up to 1200 pC N⁻¹) than PZT have already been obtained, with simultaneously lower Curie temperature ($T_c = 50\text{--}110\text{ }^\circ\text{C}$).^[32,35,40,41]

We show in this work how the geometric structure and mechanical properties can affect the piezoelectric properties using BCZT auxetic and honeycomb unit cells. The structural θ angle was varied between -35° and 35° , with negative angles leading to negative Poisson's ratios (auxetic structure) and positive angles to positive Poisson's ratio (honeycomb structure). The mechanical properties of the BCZT samples, Young's modulus, Poisson's ratio, as well as compressive strength were characterized by compression tests in combination with DIC and compared to finite element method (FEM) simulation. The piezoelectric properties were investigated by indirect excitation and correlated to the macrostructure and the mechanical properties.

2. Experimental Section

2.1. Fabrication

Ba_{0.85}Ca_{0.15}Zr_{0.1}Ti_{0.9}O₃ (BCZT) cellular structures were produced via an injection molding technique, described in detail in the study by Köllner et al.^[20] The auxetic and honeycomb unit cell is shown in **Figure 1**. All samples had a constant strut thickness t of 0.8 mm, height Y of 5.66 mm, width h of 4.92 mm, and depth T of 2.00 mm. Cubes with the same dimensions were used as references. For the ceramic injection molding, the positive CAD files were created by the algorithm-based OpenSCAD^[42] and stereolithography 3D printed with the Digitalwax 028 J and the resin Fusia DC700 (both: DWS S.r.l., Zanè, Italy). To get the negative molds, the positives were molded with polydimethylsiloxane (PDMS) (Elastosil M 4643 A B⁻¹, Wacker Chemie AG, München, Germany), which were used for ceramic injection molding. The feedstock of self-made BCZT by the solid-state approach^[7] contained 55 vol% solid loadings, 40 vol% paraffin wax (Granopent P, Carl Roth GmbH, Karlsruhe, Germany), and 5 vol% carnauba wax (Naturfarben, Carl Roth GmbH, Karlsruhe, Germany). The negative PDMS molds were filled with the feedstock under a moderate vacuum ($<10\text{ Pa}$) at $120\text{ }^\circ\text{C}$. The sintering and burnout of the organics were done on porous mullite substrates (Annamullit88, Compagnie de Saint-Gobain S.A., Courbevoie, France) under a normal atmosphere up to $1350\text{ }^\circ\text{C}$ for 6 h with heating and cooling rates between 0.1 and 5 K min^{-1} . Afterward, all samples were machined plane parallel using a pot grinder MPS 2 R220 (G&N GmbH, Erlangen, Germany) and a diamond grinding disk of $15\text{ }\mu\text{m}$. The phase composition of the powder, and sintered samples, was analyzed via X-ray diffraction (D8 ADVANCE eco, Bruker Corporation, Billerica, USA) and confirmed phase-pure BCZT in both cases, shown in **Figure 2**.

2.2. Characterization

The structural parameters Y (height), W (width), and D (depth) were measured on 15 samples per angle using a caliper. The strut

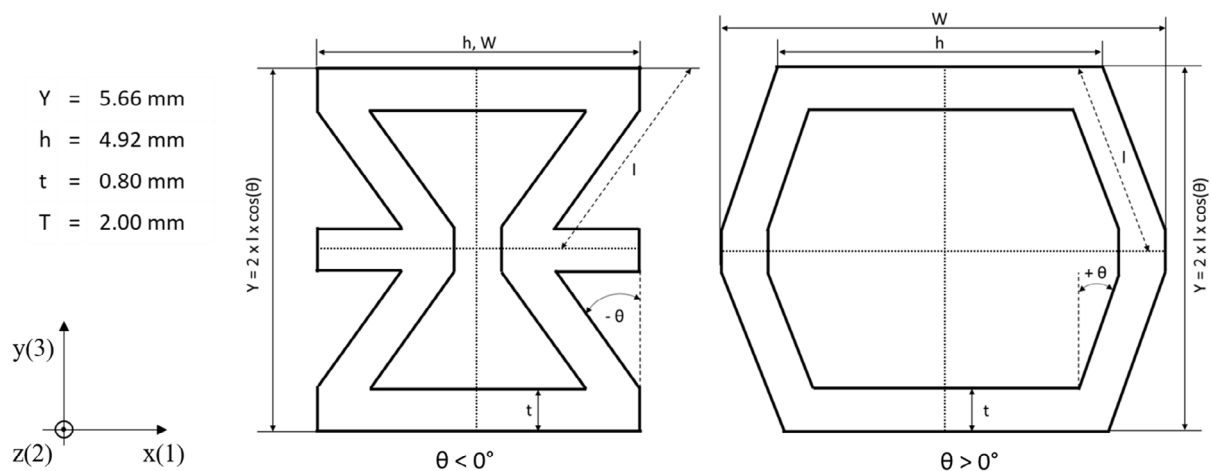


Figure 1. Auxetic ($\theta < 0^\circ$) and honeycomb ($\theta \geq 0^\circ$) unit cell with symmetry axes and structural parameters: Y : height, h : width, t : strut thickness, T : depth, l : leg length, θ : angle.

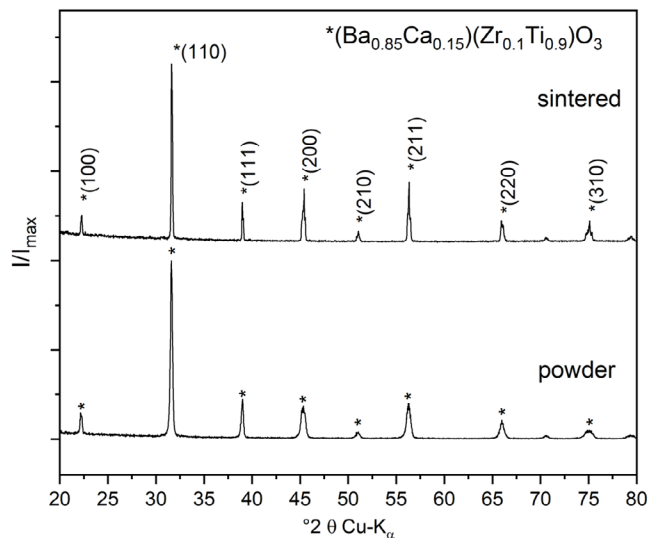


Figure 2. XRD pattern of BCZT powder and sintered sample with Miller's indices.

thickness t and the angle θ were analyzed on light microscopic images with ImageJ.^[43] The mechanical properties, compressive strength, Young's modulus, and Poisson's ratio were determined using compression tests in y -direction (Instron 5565, 5 kN load cell, 0.5 mm min⁻¹ crosshead speed, Instron Corp., High Wycombe, UK) in combination with the Ximea xiC MC089MG-SY-UB (Ximea GmbH, Münster, Germany) high-speed camera with a 0,75× TML objective lens (Edmund Optics Inc, Barrington, USA) to record the measurement with 20 frames per second. The X and Y strain was determined with ImageJ from the recordings to calculate the Poisson's ratio. Young's modulus, flexural strength, compressive strength, and density of pure BCZT were determined according to the DIN EN 843-2,^[44] DIN EN 843-1,^[45] DIN Norm 51 104,^[46] and DIN EN 623-2^[47] on bars ($26 \times 2.6 \times 2.5$ mm³) and cylinders ($\varnothing = 4.5$ mm, $h = 8$ mm). The piezoelectric constants d_{33} , d_{31} , and the relative permittivity ϵ_r were measured by the Berlincourt method (Piezo-Meter PM 300, Piezo Test, London, England) with 10 N preload and a dynamic load of 0.25 N at 110 Hz.

2.3. FEM Simulation

The FEM simulations were performed with strictly linear elastic calculations in the open-source software FreeCAD.^[48] The experimentally determined values of the reference were used as material parameters ($E = 75.24$ GPa, $\nu = 0.3$, $\rho = 5.73$ g cm⁻³). As the only boundary condition, all points with $Y = 0$ were specified as static. To determine the surface tension or strain, a force of 10 N (as in the Berlincourt measurement) or a strain of 0.1 was applied in Y -direction to the surface of Y_{\max} .

3. Results and Discussion

3.1. Macrostructure Characterization and Accuracy

Ceramic honeycomb's effective properties are very sensitive to geometric parameter variations, as described in the models of

Gibson and Ashby (Equation (2) and (3)). All geometric parameters were determined, as shown in Figure 3. The height of the unit cells is 5.87 ± 0.06 mm on the median, corresponding to an accuracy of 96%, as shrinkage and postprocessing have to be considered in the initial design. The strut thickness t (0.87 ± 0.02 mm) and width W have the lowest accuracies with 92%. The most precise parameter with 99% accuracy is the depth T of 2.02 ± 0.02 mm. However, the most relevant parameter in this work is the structural angle θ , which could be produced with an accuracy of $\pm 0.49^\circ$. On average, the relative density of the BCZT samples is only 0.03 lower than the theoretically designed values and ranges from 0.51 ± 0.03 at -35° to 0.30 ± 0.01 at 35° . The deviation in geometry results from partly manual manufacturing and postprocessing. Nevertheless, the combination of polymer 3D printing and ceramic injection molding is well suited to produce precise 2D cellular prototypes.

3.2. Influence of the Structural θ Angle on the Mechanical Properties

The mechanical properties, compressive strength σ_c , effective Young's modulus E_{eff} , and the Poisson's ratio ν of BCZT honeycombs were determined by compression tests and image analysis, shown in Figure 4. The highest compressive strength (Figure 4a) of 94.60 ± 21.72 MPa was obtained at an angle of 0° . From the maximum, the compressive strength falls in both directions to 8.57 ± 0.69 MPa at -35° and 0.91 ± 0.22 MPa at 35° . Overall, the values are consistent with the Gibson and Ashby model from Equation (2), for which the measured geometry parameters and the compressive strength of dense references ($\sigma_0 = 487.26$ MPa) were used. Only in the auxetic range (-25° to -10°) does the model underestimate the compressive strengths. The issue has already been observed on alumina auxetic and honeycomb structures, where this effect was due to the different mechanical stress modes between auxetic and honeycomb specimens.^[20] Especially the stress-excessive points showed compressive stresses in the auxetic case and tensile stresses in the honeycomb case, which lead to higher strength for the auxetic specimens.^[20,49,50]

$$\sigma_c = \sigma_0 * \left(\frac{t}{l}\right)^2 * \frac{1}{3\left(\frac{t}{l} + \sin \theta\right) \sin \theta} \quad (2)$$

The effective Young's modulus E_{eff} of the BCZT auxetic and honeycomb structures are plotted against the θ angle in Figure 4b and starts with 1.45 ± 0.51 GPa at -35° . Subsequently, Young's modulus rises to the maximum of 5.20 ± 0.35 GPa at 0° before falling to the minimum of 0.22 ± 0.02 GPa at 35° . In comparison, the linear FEM simulation starts with 3.59 GPa at -35° , reaches the maximum at -15° with 4.80 GPa, and falls afterward to 1.35 GPa at 35° . Overall, the curve progression of the FEM simulations agrees with the results of Carneiro et al.^[30] They evaluated the effective Young's modulus in the linear elastic region via compression tests on metallic 3D structures depending on the θ angle and obtained a maximum between -20 and -10° . This is in contrast with the assumption that Young's modulus decreases with lower relative density. For instance, at an angle of -30° and 15° , the BCZT unit cells show an almost identical

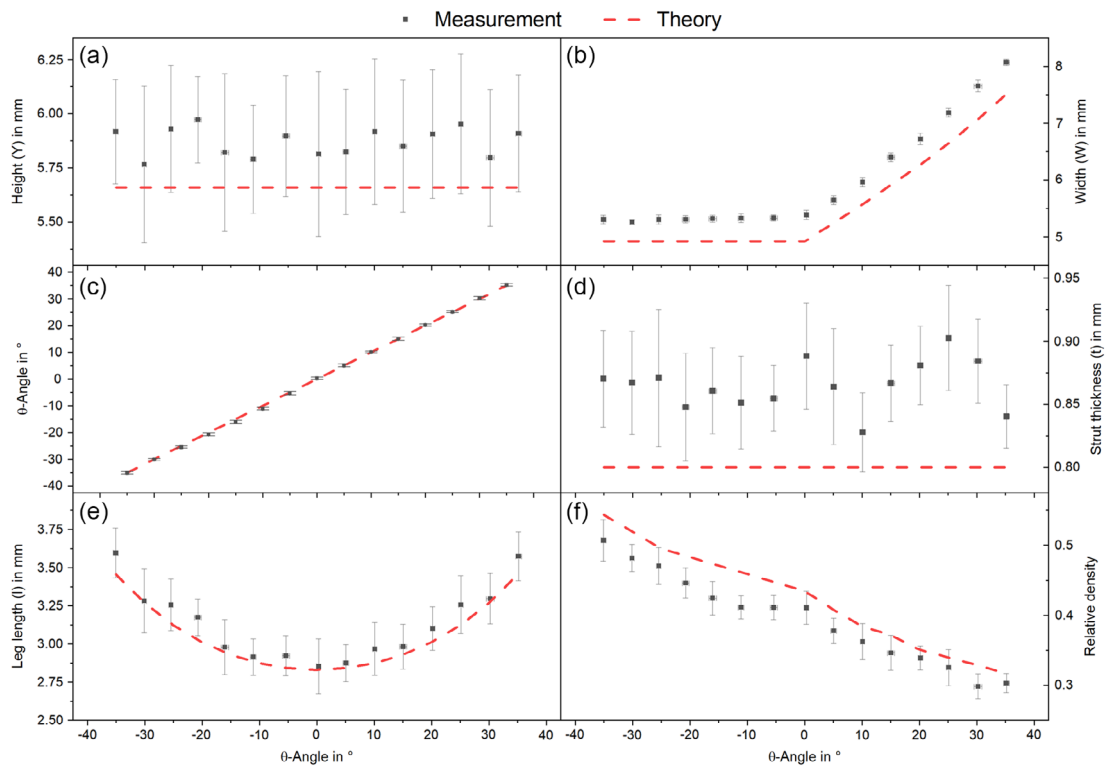


Figure 3. Structural parameters of the BCZT unit cells, a) height (Y), b) width (W), c) structural angle (θ), d) strut thickness (t), e) leg length (l), and f) relative density.

E_{eff} of 2.56 ± 0.39 GPa and 2.57 ± 1.17 GPa, but drastically different relative densities of 0.48 ± 0.02 and 0.35 ± 0.03 . This is due to the auxetic effect with negative angles, which simultaneously leads to densification and stiffening.^[30,51] The relation between relative density and E_{eff} of honeycombs was shown by Balawi et al. on only constant angles.^[28] By increasing the strut thickness, they raised the relative density and, thus, the effective modulus of elasticity. Consequently, the angle or design is more important than the relative density to optimize Young's modulus while maintaining the same weight.

However, the differences between the measured Young's modulus and the FEM simulation are due to the manufacturing variations, measuring conditions, and simplified linear FEM calculations. Even if the FEM values show x -shift plus 10° , the simulations are still a good approximation to the measured values.

The Poisson's ratios were calculated from the X and Y strains, determined from the compression test images via DIC. Figure 4c shows the Poisson's ratios depending on the θ angle for the measurement and the comparison with the FEM simulation and Gibson and Ashby model (Equation (3)). The Poisson's ratio starts with -1.26 at -35° and decreases with an increasing angle to the minimum of -2.17 at -20° . Subsequently, Poisson's ratio rises to its maximum of 1.52 at 15° and drops to 0.71 at 35° . These results are in excellent agreement with the FEM simulation, whose extrema are -1.90 and 1.82 even at -20° and 15° and differ from the measured values by only 0.3 . The model of Gibson and Ashby underestimates Poisson's ratio and only has minima and maxima of -1.16 and 0.68 . This could be because the

Young's modulus is not considered in the model since and only the geometric parameters are used for the calculation (Equation (3)).^[21] Furthermore, the theoretical model is intended for lattices, not unit cells, as used here.^[21] In comparison, the FEM simulations consider the Young's modulus and the overall dimensions, which is why they can be used more flexible even for more complex or undefined structures.^[52] Moreover, the measured values prove that the Poisson's ratio can be defined and precisely adjusted over a wide range via the θ angle.

$$\nu_{12} = \frac{\cos^2 \theta}{\left(\frac{h}{l} + \sin \theta\right) \sin \theta} * \frac{1 - \left(\frac{h}{l}\right)^2}{1 + \left(\frac{h}{l}\right)^2 \cot^2 \theta} \quad (3)$$

As the surface conditions can affect the effective piezoelectric response,^[53] the mechanical surface stresses were also analyzed via FEM using a comparison stress criteria, as shown in Figure 5. Applying a force of 10 N resulted in two maxima at 0.8 and 4.1 mm of 10.5 MPa and a maximum of 6.9 MPa in the middle of the surface at an angle of -35° . As the angle increases, the two outer peaks decrease at the same position while the center peak increases. From -25° , the stress at the center peak has the maximum value. Above 25° , the outer peaks disappear and the center peak reaches a surface stress of 25.3 MPa until 35° , whereas the reference only has a stress of 0.99 MPa (not shown). The evolution of the surface stress with increasing θ angle shows, on the one hand, a more homogeneous stress distribution in the auxetic region and, on the other hand, higher absolute stress in the honeycomb area. This also correlates with the fracture behavior of

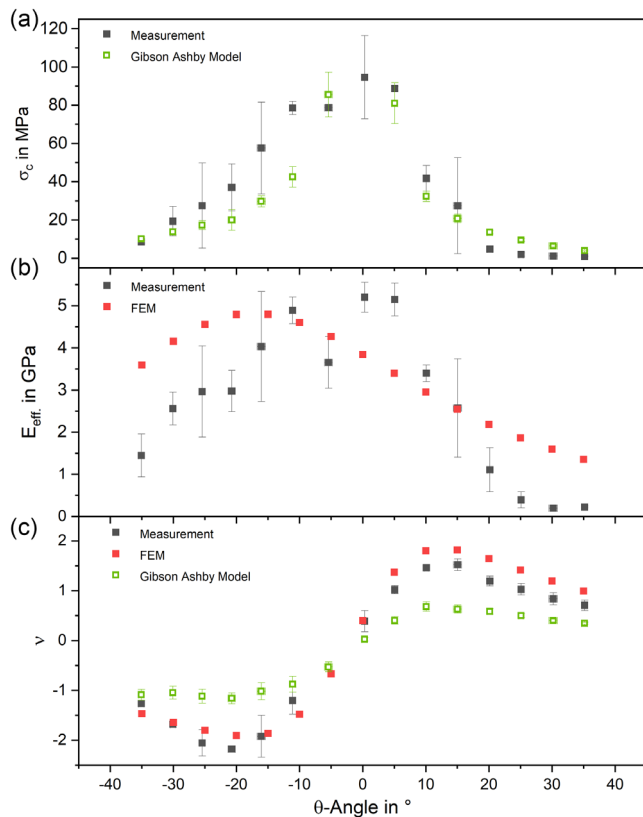


Figure 4. Mechanical properties of the BCZT unit cells dependent on the θ angle, a: compressive strength (σ_c), b: effective Young's modulus (E_{eff}), and c: Poisson's ratio (ν).

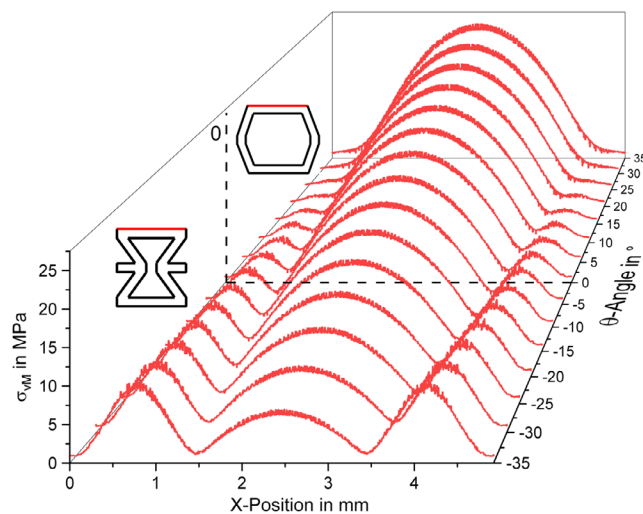


Figure 5. FEM simulations of the von Mises stress σ_{vM} (comparison stress criteria) on the surface depending on the X-position of the unit cells with an angle between -35° and 35° .

ceramic honeycombs, as described by Köllner et al.^[20] Thus, the honeycomb specimen mainly exhibited the fracture in the center of the upper strut, which is consistent with the

stress-exceeded point of this FEM simulation. Furthermore, this simulation indicates or explains that auxetic structures achieve higher strength values than honeycomb structures. Since surface defects mainly limit the strength, homogeneous stress distribution and low surface stress are desired.

3.3. Macrostructural Influence on the Piezoelectric Properties

For the classification of the piezoelectric properties, dense references with the same outer dimensions were fabricated from BCZT and measured using the Berlincourt method. The reference had a d_{33} of $191.33 \pm 24.51 \text{ pC N}^{-1}$, relative permittivity of $\epsilon_{\text{sl}} = 2371.34 \pm 77.27$, and $g_{33} = 0.009 \pm 0.001 \text{ V m N}^{-1}$. **Figure 6a** shows the piezoelectric charge coefficient d_{33} of the BCZT structures as a function of the θ angle. At an angle of -35° , the d_{33} is $196.05 \pm 30.58 \text{ pC N}^{-1}$ and then rises irregularly to the maximum value of $296.31 \pm 41.27 \text{ pC N}^{-1}$ at 5° until it falls nonlinearly to the minimum of $180.17 \pm 31.00 \text{ pC N}^{-1}$ at 35° . Unexpectedly, all BCZT auxetic and honeycomb structures except 35° have a higher d_{33} than the reference. At the maximum at 5° , d_{33} is even increased by 53% at a relative density of 0.38 (porosity of 62%). In contrast, many publications have already shown that the piezoelectric properties decrease with increasing porosity due to reduced polarization and increased content of the piezopassive phase.^[9–12,54] However, anisotropic cellular ceramics produced by freeze casting show significantly improved piezoelectric properties and have already achieved d_{33} values over 300 pC N^{-1} with a porosity of 80% (PZT), demonstrating that the macrostructure can have a major influence.^[55–58] Despite the cellular structure, the BCZT honeycomb structures as well as the auxetic structures in this work exhibit further improvement in the piezoelectric charge coefficient and even exceed it compared with the dense material. This could be due to the dense struts, which prevent the electric field from weakening at the pores or scattering. Consequently, there is a higher polarization of the material and, thus, a better piezoelectric response. Nevertheless, this would only explain equal values and no improvement. If the FEM simulations of the surface tension are included, it becomes evident that this is highly increased compared to the reference. This additional mechanical stress can generate more charges at the surface, which lead to an increased d_{33} . To further investigate the influence of the surface stresses, additional surface structuring could be generated,^[59] which could lead to a higher surface area and charge simultaneously.

The direct influence of the Poisson's ratio on d_{33} is apparent. Thus, the auxetic ($\theta < 0^\circ$) samples show a smaller average value of 221.21 pC N^{-1} than the honeycombs ($\theta \geq 0^\circ$) with 243.15 pC N^{-1} . The only exception is 35° , which deviates from the extremely low mechanical load-bearing capacity. One reason for this behavior could be dissipated mechanical energy. Bezazi et al. showed that auxetic cellular structures dissipate more energy during cyclic excitation than regular ones.^[60] In addition to the cyclic measurement via the Berlincourt method, indirect measurements by applying an electric field are currently carried out to circumvent this effect and investigate the structure's influence on d_{33} more intensely.

The influence of the θ angle on the permittivity is visible in **Figure 6b**. Here the relative permittivity of 658.29 ± 37.90 at

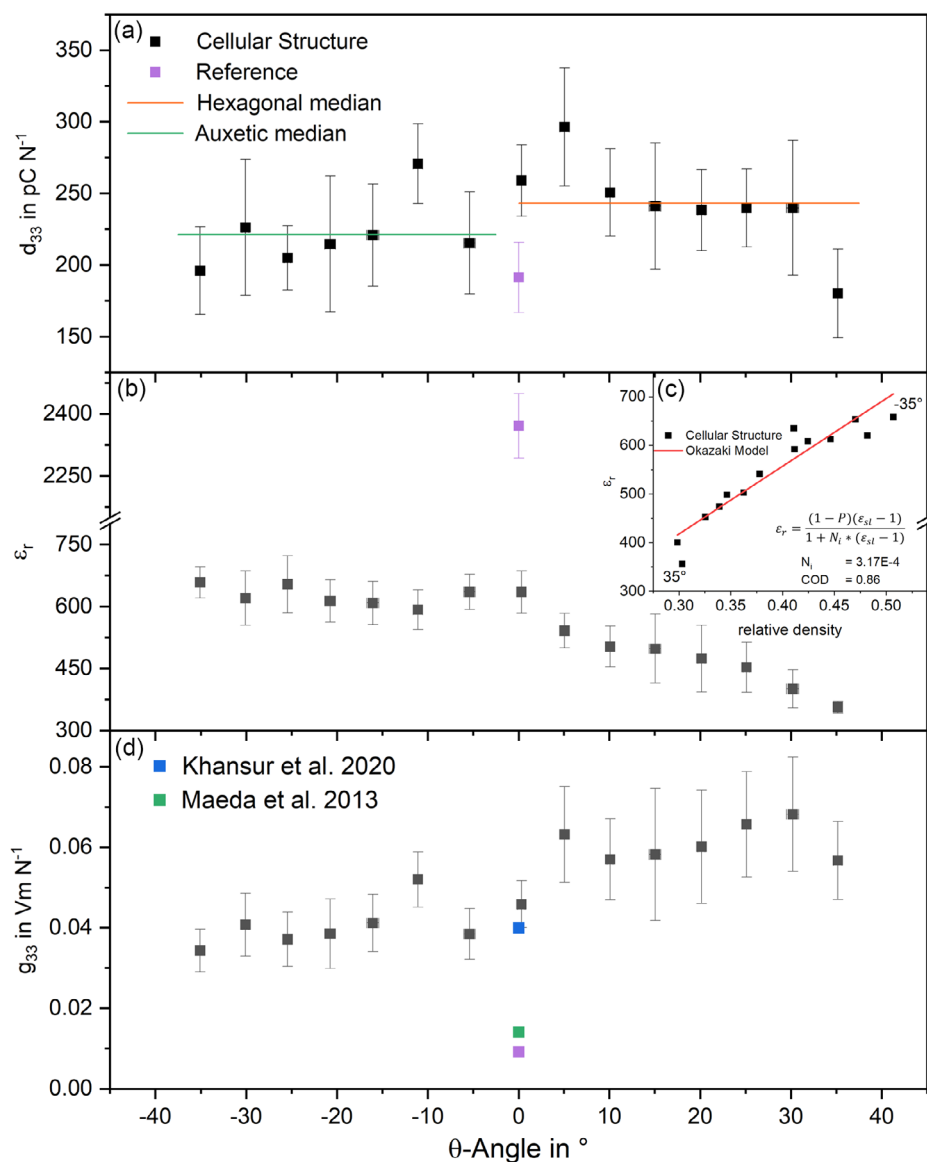


Figure 6. Piezoelectric properties of the BCZT unit cells depending on the θ -angle: a) piezoelectric charge coefficient (d_{33}), b,c) relative permittivity (ϵ_r), and d) piezoelectric voltage coefficient (g_{33}).

-35° almost linearly decreases to 256.41 ± 13.81 at 35° . As an explanation, the model from Equation (4) of Okazaki et al. can be applied, where the relative permittivity is determined from the relative density $(1-P)$, the permittivity of the material (ϵ_{sl}), and a depolarization factor (N_i).^[61] Figure 6c shows the fitted model, where the linear relationship between relative density and permittivity is evident, and a depolarization factor N_i of 0.0003 is obtained. In comparison, isotropic cellular ceramics in the same porosity range of 50–70% have N_i of around 0.002–0.004,^[13,61] a difference by a factor of 10. This results in a significantly better polarization capability of the BCZT auxetic and honeycomb structures, which explains, on the one hand, the relatively high permittivity and, on the other hand, the high d_{33} values.

$$\epsilon_r = \frac{(1-P)(\epsilon_{sl}-1)}{1+N_i*(\epsilon_{sl}-1)} \quad (4)$$

$$g_{33} = \frac{d_{33}}{\epsilon} \quad (5)$$

To characterize the efficiency of a piezoelectric device in the field of energy harvesting, the transduction coefficient ($=d_{33} * g_{33}$) is an essential figure of merit.^[11,62] The required piezoelectric stress coefficient g_{33} is calculated using Equation (5), and the results are plotted against the θ angle in Figure 6d. Beginning from the minimum g_{33} of $0.034 \pm 0.005 \text{ Vm N}^{-1}$ at -35° , it increases with the θ angle to $0.068 \pm 0.014 \text{ Vm N}^{-1}$ at 30° . Due to the indirect proportional relationship, this corresponds to the opposite trend of the relative permittivity.

The higher d_{33} values of positive θ angles reinforce the increase in g_{33} too. As a comparison, Maeda et al. obtained a g_{33} of 0.014 Vm N^{-1} with barium titanate foams at a porosity of 23%^[14] and Khansur et al. 0.04 Vm N^{-1} for PZT foams at porosities between 40 and 50%.^[11] These values are exceeded in this work with the BCZT auxetic and honeycomb structures. Despite the lower g_{33} of dense BCZT (0.009 Vm N^{-1}) compared to dense PZT (0.027 Vm N^{-1}),^[11] the g_{33} increases from dense to 50% porous PZT by a factor of 1.5, whereas BCZT structures ($\theta = -35^\circ$) by a factor of 3.8. Consequently, the structure has a greater influence on the g_{33} than porosity or material. The further increase in g_{33} of BCZT structures up to a factor of 7.5 ($\theta = 30^\circ$) can be explained by the higher porosity of up to 70%. Nevertheless, the BCZT specimens with θ angle between -15° and 5° also exhibit better mechanical strengths (58–95 MPa) than the PZT samples, which could only be loaded up to 50 MPa, although they have a lower porosity. For possible applications, both the mechanical and piezoelectric properties are elementary. In both areas, ceramic auxetic and honeycomb structures show better properties than conventional porous ceramics and can consequently be used without loss of performance while saving weight simultaneously.

4. Conclusion

Mechanical and piezoelectric properties of BCZT honeycombs have been investigated depending on the macrostructural geometry in this work. The results of compressive strength and Poisson's ratio show a strong dependence on the structural θ angle. With smaller absolute angles, they offer a significant increase in strength with a maximum at 0° of $96.4 \pm 21.7 \text{ MPa}$. Poisson's ratio could be adjusted by the θ angle from -2.2 to 1.5 . Additional FEM simulations demonstrated the relationship between increasing surface stresses, reflected in decreasing compressive strengths and increasing d_{33} values. Okazaki's model showed that auxetic and honeycomb structures could be polarized more efficiently than isotropic porous ceramics, leading to a significant improvement in piezoelectric properties. The highest d_{33} of $296.31 \pm 41.27 \text{ pC N}^{-1}$ was determined at 5° and g_{33} of $0.068 \pm 0.014 \text{ Vm N}^{-1}$ at 30° . The combination of relatively high mechanical strength and piezoelectric properties indicates the enormous potential of ceramic honeycombs to optimize sensor and energy harvesting systems.

Acknowledgements

Financial support of the German Research Foundation (DFG) in the framework of the International Research and Training Group GRK 2495 is gratefully acknowledged.

Open Access funding enabled and organized by Projekt DEAL.

Conflict of Interest

The authors declare no conflict of interest.

Data Availability Statement

The data that support the findings of this study are available from the corresponding author upon reasonable request.

Keywords

ceramic injection molding, lead-free ceramics, piezoelectric honeycombs

Received: September 22, 2022

Revised: October 26, 2022

Published online: November 17, 2022

- [1] K. Boumchedda, M. Hamadi, G. Fantozzi, *J. Eur. Ceram. Soc.* **2007**, 27, 4169.
- [2] S. Marselli, V. Pavia, C. Galassi, E. Roncari, F. Craciun, G. Guidarelli, *J. Acoust. Soc. Am.* **1999**, 106, 733.
- [3] A.-K. Yang, C.-A. Wang, R. Guo, Y. Huang, *Appl. Phys. Lett.* **2011**, 98, 152904.
- [4] C. Bowen, A. Perry, A. Lewis, H. Kara, *J. Eur. Ceram. Soc.* **2004**, 24, 541.
- [5] W. Wersing, K. Lubitz, J. Mohaupt, *Ferroelectrics* **1986**, 68, 77.
- [6] E. Mancuso, L. Shah, S. Jindal, C. Serenelli, Z. M. Tsikriteas, H. Khanbareh, A. Tirella, *Mater. Sci. Eng., C* **2021**, 126, 112192.
- [7] H. Sugimoto, J. Biggemann, T. Fey, P. Singh, D. Khare, A. K. Dubey, K. Kakimoto, *Mater. Lett.* **2021**, 297, 129969.
- [8] Q. Wang, Q. Chen, J. Zhu, C. Huang, B. W. Darvell, Z. Chen, *Mater. Chem. Phys.* **2008**, 109, 488.
- [9] F. Eichhorn, J. Biggemann, S. Kellermann, A. Kawai, K. Kato, K. Kakimoto, T. Fey, *Adv. Eng. Mater.* **2017**, 19, 1700420.
- [10] F. Eichhorn, K. Kakimoto, P. Greil, T. Fey, *Adv. Eng. Mater.* **2019**, 21, 1900390.
- [11] N. H. Khansur, J. Biggemann, M. Stumpf, K. Riess, T. Fey, K. G. Webber, *Adv. Eng. Mater.* **2020**, 22, 2000389.
- [12] J.-F. Li, K. Takagi, M. Ono, W. Pan, R. Watanabe, A. Almajid, M. Taya, *J. Am. Ceram. Soc.* **2003**, 86, 1094.
- [13] T. Zeng, X. Dong, S. Chen, H. Yang, *Ceram. Int.* **2007**, 33, 395.
- [14] K. Maeda, I. Fujii, K. Nakashima, G. Fujimoto, K. Suma, T. Sukigara, S. Wada, *J. Ceram. Soc. Jpn.* **2013**, 121, 698.
- [15] B. Praveenkumar, H. H. Kumar, D. K. Kharat, *Bull. Mater. Sci.* **2005**, 28, 453.
- [16] B. A. Tuttle, P. Yang, J. H. Gieske, J. A. Voigt, T. W. Scofield, D. H. Zeuch, W. R. Olson, *J. Am. Ceram. Soc.* **2001**, 84, 1260.
- [17] H. Lu, C.-W. Bark, D. Esque de los Ojos, J. Alcalá, C. B. Eom, G. Catalan, A. Gruverman, *Science* **2012**, 336, 59.
- [18] T. Fett, D. Munz, G. Thun, *Ferroelectrics* **2000**, 247, 321.
- [19] J. F. Nye, *Physical Properties of Crystals: Their Representation by Tensors and Matrices*, Clarendon Press, Oxford **1976**.
- [20] D. Köllner, B. Tolve-Granier, S. Simon, K. Kakimoto, T. Fey, *Materials* **2022**, 15, 2361.
- [21] L. J. Gibson, M. F. Ashby, *Cellular Solids*, Cambridge University Press, Cambridge, England **1997**.
- [22] T. Fey, F. Eichhorn, G. Han, K. Ebert, M. Wegener, A. Roosen, K. Kakimoto, P. Greil, *Smart Mater. Struct.* **2016**, 25, 15017.
- [23] H. Tang, X. Jiang, L. Li, L. Ling, Y. Hu, *J. Am. Ceram. Soc.* **2021**, 104, 2628.
- [24] H. Tang, X. Jiang, L. Ling, L. Li, Y. Hu, *J. Am. Ceram. Soc.* **2020**, 103, 6330.
- [25] S. Iyer, M. Alkhader, T. A. Venkatesh, *J. Am. Ceram. Soc.* **2014**, 97, 826.

- [26] Y. Zeng, L. Jiang, Y. Sun, Y. Yang, Y. Quan, S. Wei, G. Lu, R. Li, J. Rong, Y. Chen, Q. Zhou, *Micromachines* **2020**, *11*, 713.
- [27] J. Shi, A. H. Akbarzadeh, *Acta Mater.* **2019**, *163*, 91.
- [28] S. Balawi, J. L. Abot, *Compos. Struct.* **2008**, *84*, 293.
- [29] A. Bezazi, F. Scarpa, C. Remillat, *Compos. Struct.* **2005**, *71*, 356.
- [30] V. H. Carneiro, H. Puga, J. Meireles, *Compos. Struct.* **2019**, *226*, 111239.
- [31] <https://sdgs.un.org/goals#goals> (accessed: 2022).
- [32] J. Rödel, K. G. Webber, R. Dittmer, W. Jo, M. Kimura, D. Damjanovic, *J. Eur. Ceram. Soc.* **2015**, *35*, 1659.
- [33] Y. Saito, H. Takao, T. Tani, T. Nonoyama, K. Takatori, T. Homma, T. Nagaya, M. Nakamura, *Nature* **2004**, *432*, 84.
- [34] K. G. Webber, M. Vögler, N. H. Khansur, B. Kaeswurm, J. E. Daniels, F. H. Schader, *Smart Mater. Struct.* **2017**, *26*, 63001.
- [35] D. Ando, K. Kakimoto, *J. Am. Ceram. Soc.* **2018**, *101*, 5061.
- [36] J. Hao, W. Bai, W. Li, J. Zhai, *J. Am. Ceram. Soc.* **2012**, *95*, 1998.
- [37] M. Maraj, W. Wei, B. Peng, W. Sun, *Materials* **2019**, *12*, 3641.
- [38] X. Yan, M. Zheng, Y. Hou, M. Zhu, *J. Eur. Ceram. Soc.* **2017**, *37*, 2583.
- [39] T. Samma, T. Fuchigami, S. Nakamura, T. Fey, K. Kakimoto, *Phys. Status Solidi (B)* **2022**, *259*, 2100611.
- [40] W. Liu, X. Ren, *Phys. Rev. Lett.* **2009**, *103*, 257602.
- [41] M. C. Ehmke, S. N. Ehrlich, J. E. Blendell, K. J. Bowman, *J. Appl. Phys.* **2012**, *111*, 124110.
- [42] OpenSCAD, <https://openscad.org/> (accessed: 2022).
- [43] ImageJ, <https://imagej.net/downloads> (accessed: 2022).
- [44] Deutsches Institut für Normung, *Hochleistungskeramik_- Mechanische Eigenschaften monolithischer Keramik bei Raumtemperatur_- Teil_2: Bestimmung des Elastizitätsmoduls, Schubmoduls und der Poissonzahl; Deutsche Fassung EN_843-2:2006*, Beuth Verlag GmbH, Berlin **2007**.
- [45] Deutsches Institut für Normung, *Hochleistungskeramik_- Mechanische Eigenschaften monolithischer Keramik bei Raumtemperatur_- Teil_1: Bestimmung der Biegefestigkeit; Deutsche Fassung EN_843-1:2006*, Beuth Verlag GmbH, Berlin **2008**.
- [46] Deutsches Institut für Normung, *Hochleistungskeramik_- Mechanische Eigenschaften monolithischer Keramik bei Raumtemperatur_- Bestimmung der Druckfestigkeit*, Beuth Verlag GmbH, Berlin **2010**.
- [47] Deutsches Institut für Normung, *Hochleistungskeramik; Monolithische Keramik; Allgemeine und strukturelle Eigenschaften; Teil_2: Bestimmung von Dichte und Porosität; Deutsche Fassung EN_623-2:1993*, Beuth Verlag GmbH, Berlin **1993**.
- [48] <https://www.freecadweb.org/> (accessed: 2022).
- [49] R. Telle, *Keramik*, Springer Berlin/Heidelberg, Berlin, Heidelberg **2007**.
- [50] X. Hou, Z. Deng, K. Zhang, *Acta Mech. Solida Sin.* **2016**, *29*, 490.
- [51] S. Malek, L. Gibson, *Mech. Mater.* **2015**, *91*, 226.
- [52] H. M. A. Kolken, A. A. Zadpoor, *RSC Adv.* **2017**, *7*, 5111.
- [53] S. Dai, M. Gharbi, P. Sharma, H. S. Park, *J. Appl. Phys.* **2011**, *110*, 104305.
- [54] J. I. Roscow, R. Lewis, J. Taylor, C. R. Bowen, *Acta Mater.* **2017**, *128*, 207.
- [55] S.-H. Lee, S.-H. Jun, H.-E. Kim, Y.-H. Koh, *J. Am. Ceram. Soc.* **2007**, *90*, 2807.
- [56] S.-H. Lee, S.-H. Jun, H.-E. Kim, Y.-H. Koh, *J. Am. Ceram. Soc.* **2008**, *91*, 1912.
- [57] J. I. Roscow, Y. Zhang, M. J. Krašny, R. W. C. Lewis, J. Taylor, C. R. Bowen, *J. Phys. D: Appl. Phys.* **2018**, *51*, 225301.
- [58] Y. Zhang, J. Roscow, M. Xie, C. Bowen, *J. Eur. Ceram. Soc.* **2018**, *38*, 4203.
- [59] J. Biggemann, D. Köllner, S. Simon, P. Heik, P. Hoffmann, T. Fey, *Ceramics* **2021**, *4*, 681.
- [60] A. BEAZI, F. SCARPA, *Int. J. Fatigue* **2007**, *29*, 922.
- [61] K. Okazaki, *Ferroelectrics* **1981**, *35*, 173.
- [62] D. R. J. Brandt, M. Acosta, J. Koruza, K. G. Webber, *J. Appl. Phys.* **2014**, *115*, 204107.